BAU Journal - Science and Technology

Volume 1 | Issue 2
ISSN: 2706-784X

Article 10

June 2020

Studies of SmBa2Cu3O7-δ / ZnFe2O4 Superconducting Composites

Hadi Basma
Assistant Professor, Faculty of Science, Beirut Arab University, Beirut, Lebanon, h.basma@bau.edu.lb

Waleed Abdeen
Assistant Professor, Faculty of science, Alexandria University, Egypt, waleed_abdeen73@yahoo.com

Ayman El-Tahan
Assistant Professor, Faculty of Science, Tanta University, Tanta, Egypt,
ayman.eltahan@science.tanta.edu.eg

El-Maghraby El-Maghraby
Professor, Faculty of Science, Damanhour University, Damanhour, Egypt, maghrabym@yahoo.com

Ahmed Khalaf
Assistant Professor, Faculty of Science, Damanhour University, Damanhour, Egypt,
a_khalaf81@yahoo.com

Studies of SmBa2Cu3O7-δ / ZnFe2O4 Superconducting Composites

Abstract

SmBa2Cu3O7-δ /(ZnFe2O4)x superconducting composites with 0.00 ≤ x ≤ 0.20 wt% were prepared by the usual solid-state reaction method. The prepared samples were investigated using X-ray powder diffraction (XRD) at room temperature and electron paramagnetic resonance (EPR) measurements in the temperature range (100-295 K). It is found that EPR spectra are dominated by an anisotropic Cu2+ EPR pattern. Moreover, the EPR spectral intensity increases as the temperature decrease from room temperature down to 100 K. The number of spins (N) participating in EPR resonance, the activation energy (Ea), the paramagnetic susceptibility (c) and the effective magnetic moment (μeff) are calculated as a function of both nanosized ZnFe2O4 addition and temperature. The results are interpreted in terms of localized Cu2+ ions from non-superconducting impurity phases and confirmed by magnetization-field (M-H) hysteresis measurements.

Keywords

SmBa2Cu3O7-δ, ZnFe2O4, electron paramagnetic resonance, number of spins.

1. INTRODUCTION

$SmBa_2Cu_3O_{7-\delta}$ (Sm-123) system is a perovskite-type ceramic superconductor. Its structure is orthorhombic for high oxygen content ($0.4 \geq \delta \geq 0$) and becomes tetragonal for $\delta > 0.4$ (Song et.al, 2004, Xue et.al, 2013). This system possesses superior superconducting properties and is capable of trapping higher magnetic fields in comparison to conventional permanent magnets (Durrel at.al, 2014, Shi et.al, 2015). These favorable characteristics allowed the exploitation of the system in applications such as quasi-permanent magnets , coated conductors and current leads (Oh et.al, 2013, Nigro et.al, 2004). Sm-123, as most HTSCs, experience a decrease in critical current density at high magnetic fields and temperature. Several studies have shown that the addition of magnetic nanoparticles to (HTSCs) plays an important role in enhancing the flux pinning and critical current density (Abdeen et al., 2016, Mohammed et al., 2016, Qu et al., 2008). A large number of EPR investigations have already been devoted to studying HTSCs (Guskos et.al, 1990, Guskos etal., 1990, Punnoose etal., 1995). The EPR of Cu^{2+} ions in cuprates superconductors have g-factor ranging from $g = 2$ to 2.4 [Dhage et al., 1995, Hoffman et al., 1998, Khan etal., 1997]. Awad et al., 2012 studied the EPR spectra at different temperatures (120-290 K) for $GdBa_2Cu_{3-x}Ru_xO_{7-\delta}$ phase. All EPR spectra consisted an isotropic EPR line. This was attributed to Gd^{3+} ions with g=2.01. The temperature dependence of EPR spectra for Gd-123 superconductors was investigated by Calamiouto et al., 2012. Two signals corresponding toGd^{3+} ions with g = 1.999(2) and Cu^{2+} ions with $g_x = 2.074$, $g_y = 2.015$ and g_z, = 2.202 were observed. Vier et al., 1987, recorded the EPR spectra of $REBa_2Cu_3O_{9-\delta}$ (RE-123, RE= Y or rare earth) superconductors at different temperatures and reported that the impurity phase $BaCuO_2$ (dark phase) is the main source of EPR signals of Cu^{2+} ions in Y-123 at low (< 40 K) temperature. Bowden et al., 1987 showed that any EPR signal in nominally pure Y-123 superconducting material is probably due to a small amount of impurity Y211 (green phase) compound**.** Koksharov et al.,1991 studied the EPR spectra for Sm-123 single crystal at a temperature range (4-290 K). At room temperature the EPR spectrum is almost isotropic with g=2.10(2) which may be related to the Cu^{2+} Jahn-Teller (JT) centers. Awad et al., 2017 conducted EPR studies of Sm-123/ $(MnFe_2O_4)_x$ composites. The EPR signal showed a dominant Cu^{2+} anisotropic pattern described by anisotropic g-factor. This EPR spectra are mainly due to the impurity phases with no evident effect of $MnFe_2O_4$ addition. Isber et al., 2017 studied the effect of the addition of nano $ZnFe_2O_4$ addition on $GdBaCu_3O_{7-\delta}$ superconducting phase before and after irradiation by 3MeV H+ ions. The magnetic properties such as the activation energy and the number of spins and showed an increase with an addition up to 0.06wt%. The superparamagnetic behavior of $ZnFe_2O_4$ was evidenced by Raita et.al, 2015 through EPR measurements in both X and Q bands. The resonance field was found to shift to lower fields and the broadening of the lined showed an increase with the decrease of temperature. In our previous work (Abdeen et.al, 2016) $ZnFe_2O_4$ addition showed a good enhancement of the superconducting and mechanical properties of Sm-123 phase so we believe that the investigation of the contribution of super paramagnetic $ZnFe_2O_4$ in the magnetic behavior of Sm-123 might be quite interesting.

In this work, the EPR studies of Sm-123/$(ZnFe_2O_4)_x$ composites is reported, with $0.00 \leq x \leq 0.20$ wt% prepared by the solid state reaction technique are investigated at different temperatures. The analysis of the EPR spectra for Sm-123/$(ZnFe_2O_4)_x$ composites allowed the determination of several EPR magnetic parameters. The variations of these parameters are discussed as a function of nanosized $ZnFe_2O_4$ addition and the temperature variation.

2. EXPERIMENTAL TECHNIQUES

The Nano ferrite (ZnFe2O4) was synthesized using the wet chemical coprecipitation method while Sm-123/ZnFe2O4 composite was synthesized suing the conventional solid-state reaction technique. The details of the preparation was reported previously (Abdeen et.al, 2016). The EPR measurements were performed using a Bruker microwave controller (ER 048 spectrometer). The spectrometer was operated at the X-band frequency (9.24 GHz) and the microwave power of 15mW. The magnetic field was scanned in the range 0–10,000 G, and recorded at a temperature range (100–295 K).

3. RESULTS AND DISCUSSION

3.1 Phase Purity and Lattice Parameters

The structural and electrical properties of Sm-123/ $ZnFe_2O_4$ was extensively investigated and reported in our previous publication (Abdeen et.al, 2016). XRD patterns of $SmBa_2Cu_3O_{7-\delta}/(ZnFe_2O_4)_x$, ($x$ = 0.00, 0.02 , 0.08, 0.15 and 0.20 wt%) are shown in **Figure 1**. The XRD patterns at room temperature of all samples reveal an orthorhombic perovskite structure with small amounts of non-superconducting phase $BaCuO_2$ (as evident by additional peak at $2\theta \approx 29^o$).

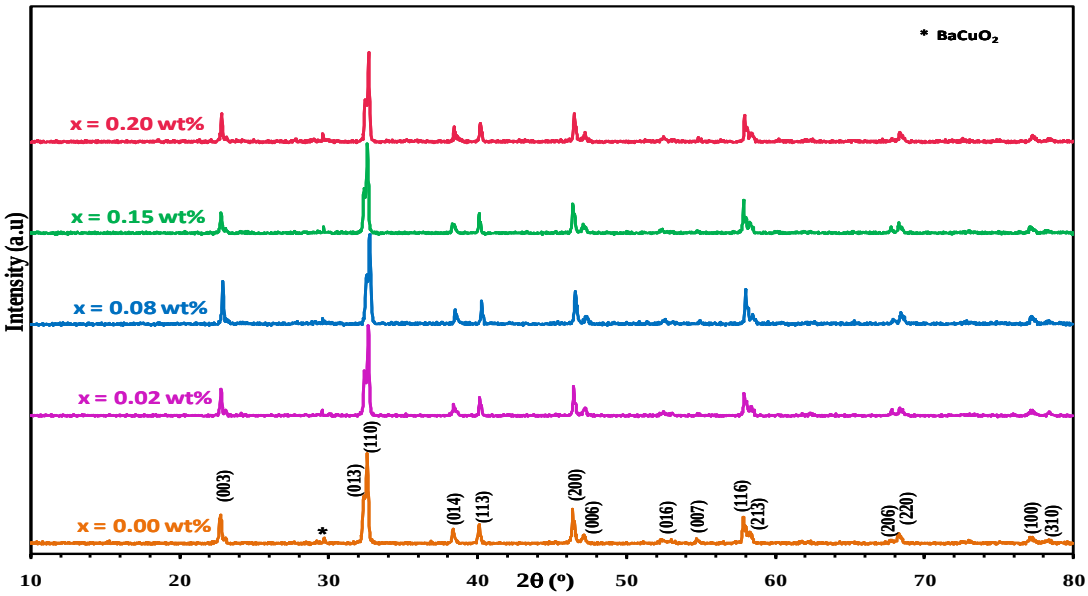

Fig.1: X-ray powder diffraction pattern for $SmBa_2Cu_3O_{7-\delta}/(ZnFe_2O_4)_x$ with x = 0.00, 0.02, 0.08, 0.15 and 0.20 wt%.

By analyzing the XRD measurements, volume fractions of Sm-123 and BaCuO2 phases are calculated and listed in Table 1. The results show that the relative volume fraction of Sm-123/(ZnFe2O4)x superconducting phase increases with x up to 0.08 wt% and then decreases with further addition. This means that the higher addition (x > 0.08 wt%) of nanosized ZnFe2O4 slightly retards the phase formation of Sm-123 and the superconducting parameters such as superconducting transition temperature (Tc) (Abdeen et.al, 2016). as shown in Table 1, whereas it enhances the BaCuO2 phase formation. The values of Tc determined from electric resistivity measurements are also reported in Table.1.The enhancement of Tc with x up to 0.08wt.% can be attributed to the increase in the superconducting volume fraction of Sm-123. Furthermore, nanosized ZnFe2O4 particles heal up the voids and pores and hence improve the weak links among the superconducting grains. The decrease of Tc for x > 0.08 wt%, might be attributed to the non-homogeneous distribution of ZnFe2O4 nanoparticles causing agglomeration and segregation at the grain boundaries of Sm-123 superconductor. The magnetic nanoparticles at grain boundaries scatter the carriers during their transport and cause pair braking. The variation of Jc (Abdeen et.al, 2016). with x shows a similar trend as Tc. The increase in Jc is attributed to both increase in the volume fraction of Sm-123 phase and the diffusion of nanosized ZnFe2O4 over the pore surfaces, grain boundaries and twin boundaries. This can improve the inter-granular coupling between grains and increase the flux pinning centers leading to enhancement of Jc.

The values of the lattice parameters a, b and c are listed in Table 1 for Sm-123/(ZnFe2O4)x superconducting composites. The lattice parameters show no systematic variation with respect to the pure sample and the structure does not change from orthorhombic to tetragonal. This result indicates that the nanosized ZnFe2O4 does not enter the crystal structure and reside on the grain boundaries.

Table 1: The relative volume fraction and lattice parameters of $SmBa_2Cu_3O_{7-\delta}/(ZnFe_2O_4)_x$, x = 0.00, 0.02, 0.08, 0.15 and 0.20 wt%.

x (wt%)	Sm-123%	$BaCuO_2$%	a(Å)	b(Å)	c(Å)	T_c
0.00	97.412	2.588	3.860	3.907	11.702	91.50
0.02	97.698	2.302	3.856	3.906	11.699	93.09
0.08	98.784	1.216	3.854	3.901	11.695	96.08
0.15	97.683	2.317	3.860	3.903	11.701	91.72
0.20	97.341	2.659	3.858	3.901	11.699	88.69

3.2 Cu2+ EPR Measurements

EPR studies of HTSCs above Tc give information on the local Cu2+ environments and their interaction with neighboring ions. The first-derivative of the EPR spectra of Sm-123 superconductor sample at different temperatures T = 295, 260, 230, 190,160, 130 and 100 K is shown in Figure.2. In the whole temperature range, the EPR spectrum comprises of a single asymmetric line described by rhombic g tensor with a slight temperature dependence. The principal g values are calculated and found in the range gx =2.073-2.077, gy =2.123-2.128 and gz= 2.194- 2.202, where the first value corresponds to (100K) and the second to (295K). The variation of the anisotropic g-values with temperature for Sm-123 pure sample is shown in Figure 3. These signals correspond to the anisotropic powder-like EPR spectrum of divalent copper ion (3d9 , electron spin s = ½ , nuclear spin I = 3/2) in non-cubic site. According to the crystal field theory the relation gz>gy>gx among the principal g-values indicates that the underlying Cu2+ centers have a dominant dx2-y2 and to a lesser extent a d_z^2 contribution in their ground state that corresponds to a rhombic distortion of the local symmetry (Likodimos et al., 1995).

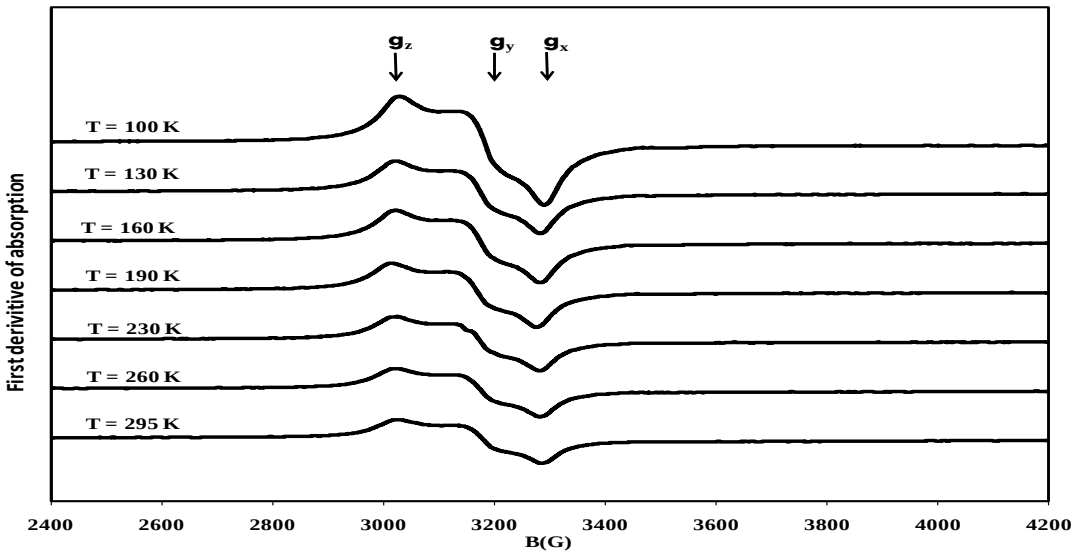

Fig.2: First-derivative absorption spectra for $SmBa_2Cu_3O_{7-\delta}$ versus the magnetic field at different temperatures.

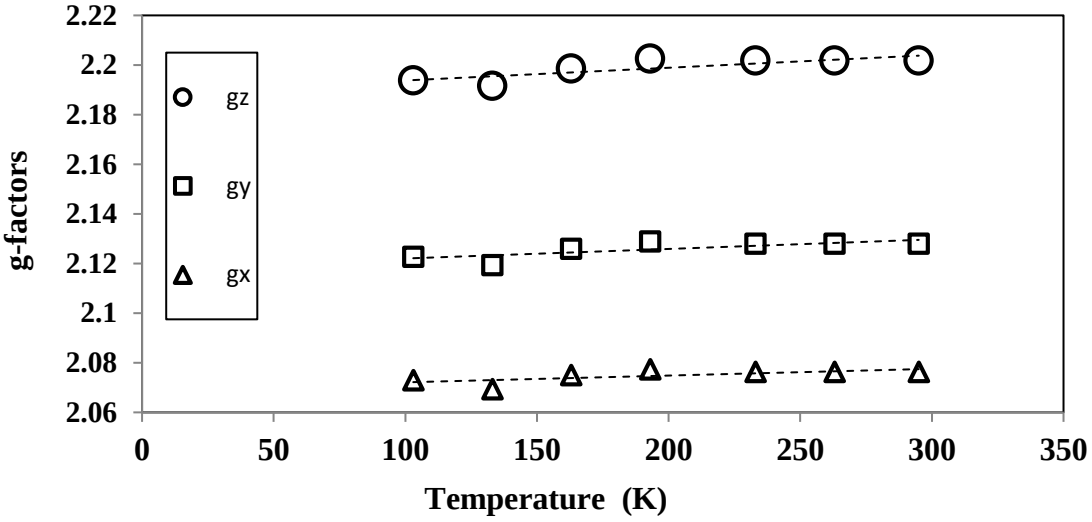

Fig.3: Variation of anisotropic g-factor with temperature for the $SmBa_2Cu_3O_{7-\delta}$.

The EPR spectra of SmBa2Cu3O7−δ/(ZnFe2O4)x composites at 100 K are shown in Figure 4. All the samples show the anisotropic EPR spectra for Cu2+ ion with different intensities. Actually, the impurity phases RE2BaCuO5 (RE-211) and BaCuO2 usually appear during the sintering of the REBa2Cu3O7-δ compounds (Bowden et al,. 1987) and both can be detected in the EPR measurements of samples (Kuang et al, 2017).

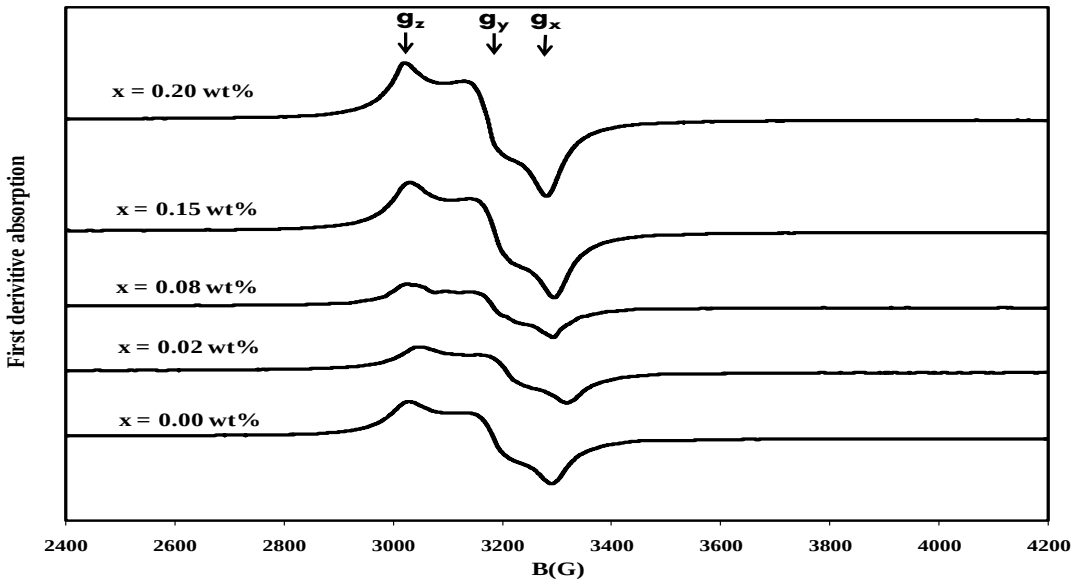

Fig.4: First-derivative absorption spectra versus magnetic field for the $SmBa_2Cu_3O_{7-\delta}$ / $(ZnFe_2O_4)_x$, with x=0.00, 0.02, 0.08, 0.15 and 0.20 wt%.

However, this only enhances its importance as a tool for the detection of Cu2+ containing impurities (Likodimos et al.,1996). From XRD measurements the impurity phases, (especially BaCuO2) reported in table 1 are typically present in the X-ray spectra of the Sm-123/(ZnFe2O4)x composites. Although the X-ray spectra show no peaks for the Sm-211 impurity phase, the presence of < 1% of this phase could contribute to the EPR signals (Vier et al., 1987). The relative EPR intensity with respect to temperature for SmBa2Cu3O7−δ/(ZnFe2O4)x composites, with $0.00 \leq x \leq 0.20$ wt% is shown in Figure 5.

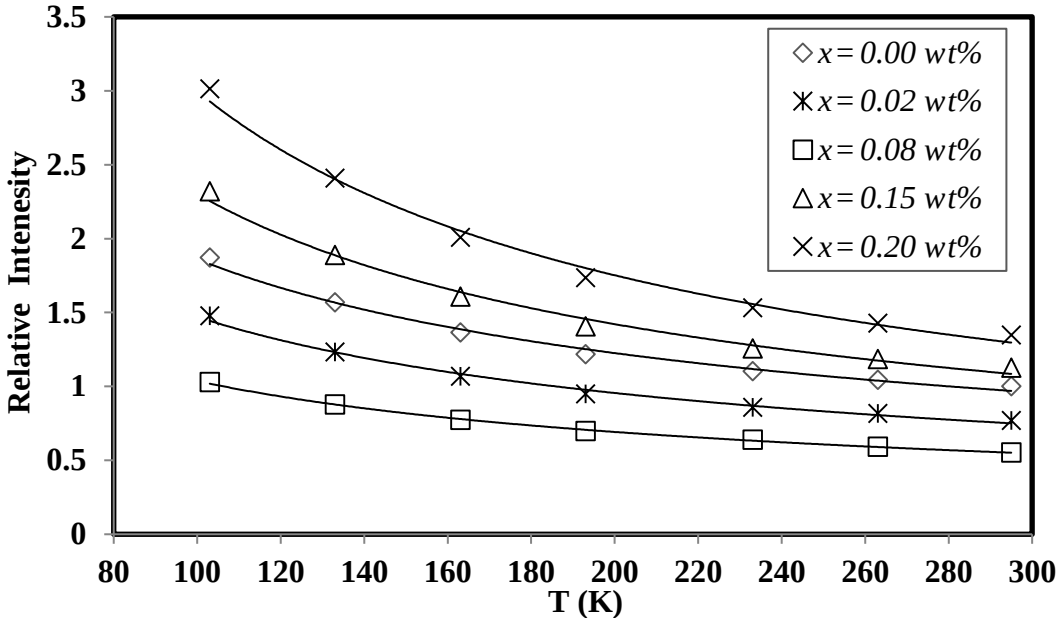

Fig.5: Variation of the EPR relative intensity with temperature for the $SmBa_2Cu_3O_{7-\delta}$ / $(ZnFe_2O_4)_x$, with x=0.00, 0.02, 0.08, 0.15 and 0.20 wt%.

The EPR relative intensity shows a decrease up to x=0.08 wt%, consistent with the XRD results that show that the impurity phase BaCuO2 is suppressed. Based on this observation, we assume that this EPR spectrum originates mainly from Cu2+ ion in the disordered part of the BaCuO2 compound (Guskos et al., 1995). At higher nanosized addition $x \geq 0.15$ wt% the increase in the EPR line intensity could not be attributed only to the impurity phase BaCuO2 but also the partial contribution from nanosized ZnFe2O4 cannot be excluded. It was reported by Jones et al., 1990 that the EPR spectra from the impurity phase BaCuO2 are easily observed. The relative EPR line intensity for SmBa2Cu3O7−δ/(ZnFe2O4)x samples decreases as the temperature increases from 100 K up to room temperature The EPR line intensity varied with temperature according to Curie–Weiss law at temperature higher than Tc which is expected for a simple paramagnetic center with spin S=1/2 as Cu2+ ions (Genossar et al., 1989). The EPR peaks shift towards low fields as the temperature decreases due to the modification in crystal field experienced by the ions. The linewidths turned out to be anisotropic, following the relation $\Delta Hz > \Delta Hy > \Delta Hx$ which is consistent with spin-spin interaction contribution to ΔH predicted by the principal g-values. Figure 6 shows the temperature dependence of linewidths ΔHz, ΔHy and ΔHx for free added sample. The linewidths show slight linear increase with the increase of temperature. This behavior may be associated with very rapid spin-lattice relaxation (Bencini et al., 2012).

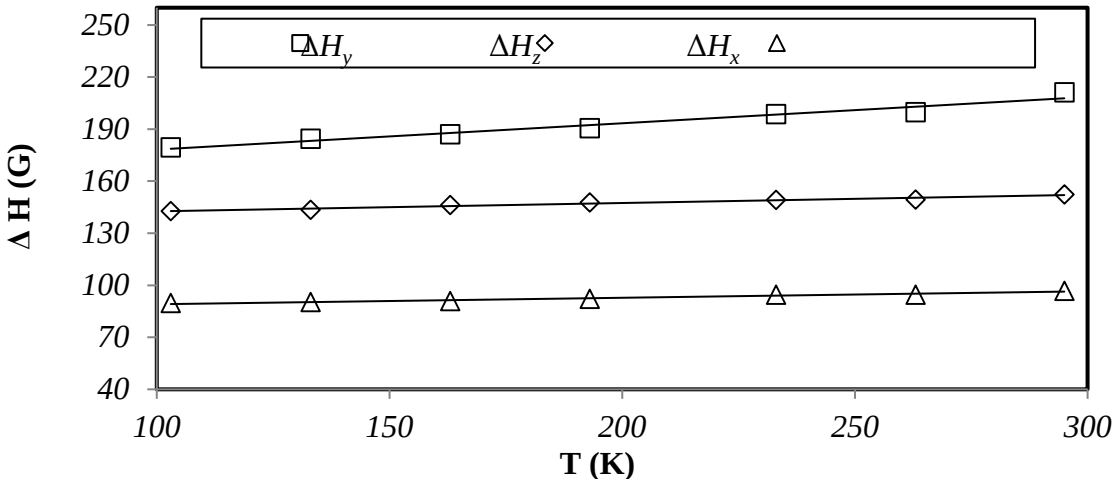

Fig.6: Variation of the linewidth ΔH with temperature for $SmBa_2Cu_3O_{7-\delta}$.

Figure 7 shows the concentration dependence of linewidths ΔHz, ΔHy and ΔHx at 100 K. As the nanosized ZnFe2O4 addition increases, the width of the resonance lines decreases up to x= 0.08 wt%, indicating that the concentration of paramagnetic ions decreases and hence, the BaCuO2 concentrations. On further addition of nanosized ZnFe2O4, the width of the resonance lines increases which means the formation of large clusters Cu2+ ions (the broad profile arising from spin pairing due to the close proximity of the paramagnetic ions).

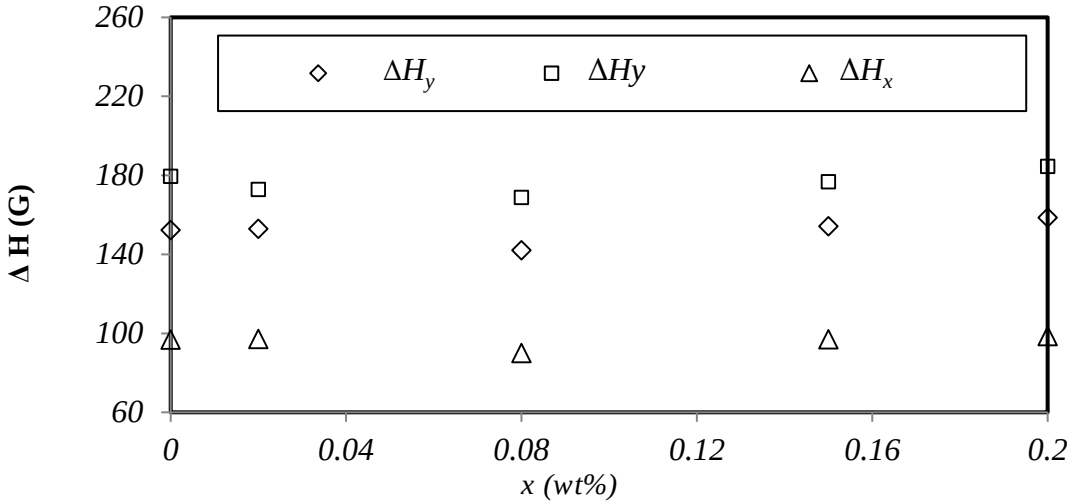

Fig.7: The concentration dependence of the linewidth ΔH for $SmBa_2Cu_3O_{7-\delta}/(ZnFe_2O_4)_x$, with x=0.00, 0.02, 0.08, 0.15 and 0.20 wt%.

The number of spins N participating in the resonance was calculated using the area under the absorption curve (Weil et al., 2007). The plot between log(N) and 1/T for Sm-123/(ZnFe2O4)x composites is shown in Figure 8. It shows a linear dependence which is compatible with Boltzmann's law. It is found that N decreases as the nanosized ZnFe2O4 addition increase up to x=0.08 wt%, and it decreases as the temperature increases. The activation energy Ea was calculated from the slope of lines, and the values of Ea are also listed in Table 2 as a function of nanosized ZnFe2O4 addition. Ea decreases as x increases up to x=0.08 wt%, and then increases with further additions. This enhancement is accordingly the consequence of increasing N with nanosized ZnFe2O4 addition for x > 0.08 wt%, consistent with the variation of the impurity phase BaCuO2.

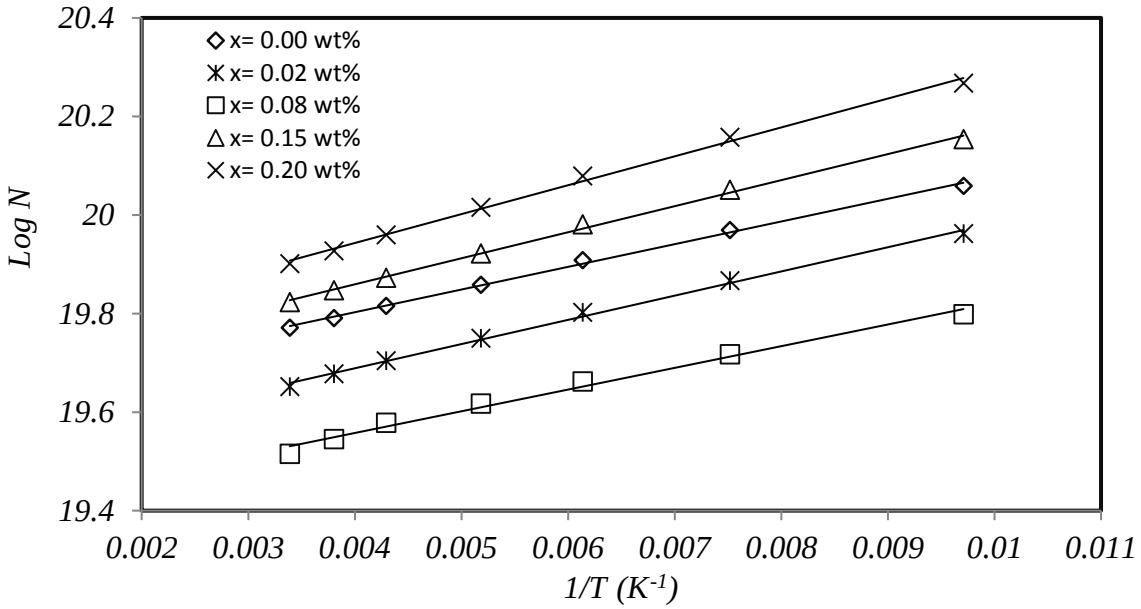

Fig.8: Relation between Log(N) and 1/T for $SmBa_2Cu_3O_{7-\delta}$ / $(ZnFe_2O_4)_x$, with x=0.00, 0.02, 0.08, 0.15 and 0.20 wt% at 100 K.

Table 2: Variation of E_a, χ_o, Θ and μ_{eff} for $SmBa_2Cu_3O_{7-\delta}$ / $(ZnFe_2O_4)_x$ with x=0.00, 0.02, 0.08, 0.15 and 0.20 wt%.

x wt%	Ea (eV)	$\chi_o \times 10^{-8}$ (emu/gm)	$\chi \times 10^{-5}$ (emu.K/gm)	Θ	μ_{eff} (μ_B)
0.00	0.0092	-6.19	6.18	49.01	**0.72**
0.02	0.0091	-5.48	5.18	45.35	**0.61**
0.08	0.0087	-4.26	3.84	43.51	**0.53**
0.15	0.0105	-8.99	7.44	51.68	**0.73**
0.20	0.0115	-11.92	9.05	55.05	**0.74**

3.3 Paramagnetic Susceptibility:

The paramagnetic susceptibility χ was determined as a function of temperature using Eq.[1] (Ashcroft at al., 1976)

Eq.(1) $$\chi = \frac{Ng^2\mu_\beta^2 J(J+1)}{3K_B T}$$

where N is the number of spins per m3, $\mu\boldsymbol{\beta}$ is Bohr magneton, kB is the Boltzmann constant and J=5/2. Figure 9 shows the temperature dependence of the paramagnetic susceptibility for the Sm-123/(ZnFe2O4)x composites. The χ–T curves were well fitted according to Curie–Weiss law, using the following equation:

Eq. (2) $$\chi = \chi_o + \frac{C}{T-\theta}$$

where χo is the temperature independent susceptibility, C is Curie constant and Θ is Curie temperature, and their values are listed in Table 2.

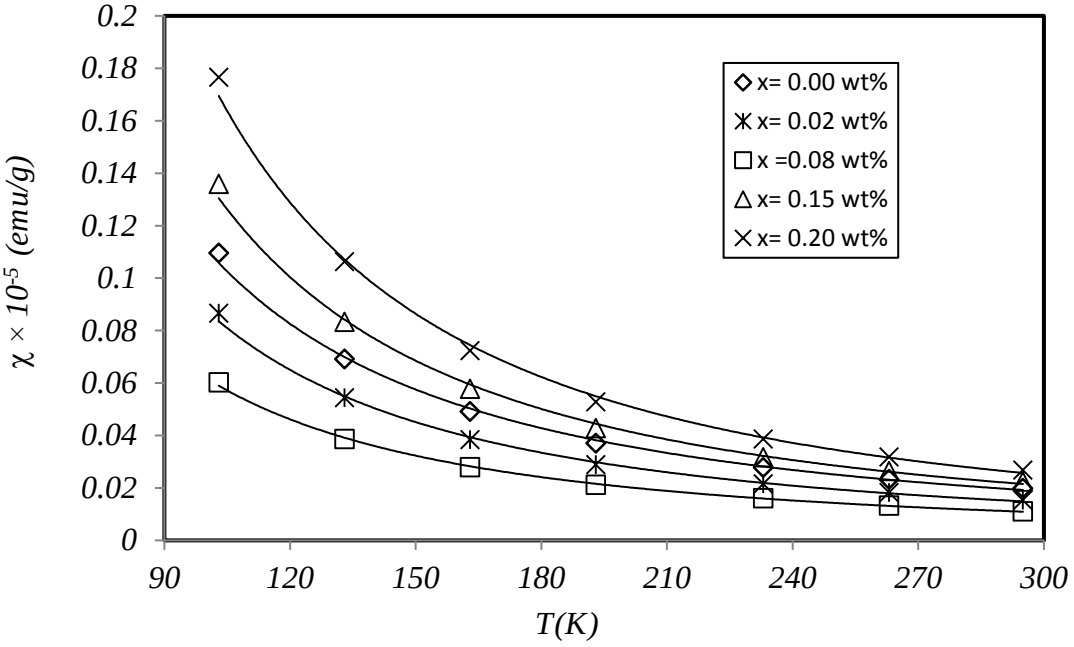

Fig.9: Temperature dependence of paramagnetic susceptibility for $SmBa_2Cu_3O_{7-\delta}$ / $(ZnFe_2O_4)_x$, with x= 0.00, 0.02, 0.08, 0.15 and 0.20 wt%.

The quantity C can be expressed as an equivalent amount of magnetic ions and the positive sign of Θ evidence for the ferromagnetic interactions between the copper paramagnetic centers whereas the negative sign of χo is the diamagnetic contribution into the susceptibility caused by the core electrons of BaCuO2 (Troc et al., 1994)
The ceffective magnetic moment μeff is calculated using Eq.(3):

Eq.(3) $$C = \frac{N\mu_{eff}^{2}}{3K_B}$$

It should be noted that the calculated μeff represents a sum of the contributions from all the sample constituents. In all of the studied samples, EPr signals corresponding to Sm3+ ions (μeff = 0.84μ**β**) are not observed. This can be attributed to very fast spin lattice in contrast with the other RE3+ Kramers ions whose EPR linewidth is mainly determined by their magnetic interactions (Likodimos et al., 1995). On the other hand, Udomkan et al., 2005 studied the EPR spectra of Gd-123 and found that the Cu2+(3d9) ions from the impurity phase BaCuO2 give rise to two-quartet absorption peaks centered at ≈310 mT (g ≈ 2.020) which are superposed by the broad ESR peak of Gd3+(4f7) at g ≈ 2.000. The values of μeff are listed in Table 2 as a function of nanosized ZnFe2O4 addition after excluding the magnetic moment resonances only due to small amount of nanosized ZnFe2O4 addition. The effective magnetic moment is found to be proportional to the amount of BaCuO2 present, which strongly suggests that BaCuO2 is the greatest contributor to the EPR signal and to the magnetic susceptibility for SmBa2Cu3O7−δ/(ZnFe2O4) x, 0.00 ≤ x ≤ 0.20 wt% above Tc. Vier et al., 1987 obtained similar results for a number of REBa2Cu3O9-δ HTSCs. Figure 10 shows the M–H curves of SmBa2Cu3O7−δ and SmBa2Cu3O7−δ/(ZnFe2O4)0.08 at 85 K.

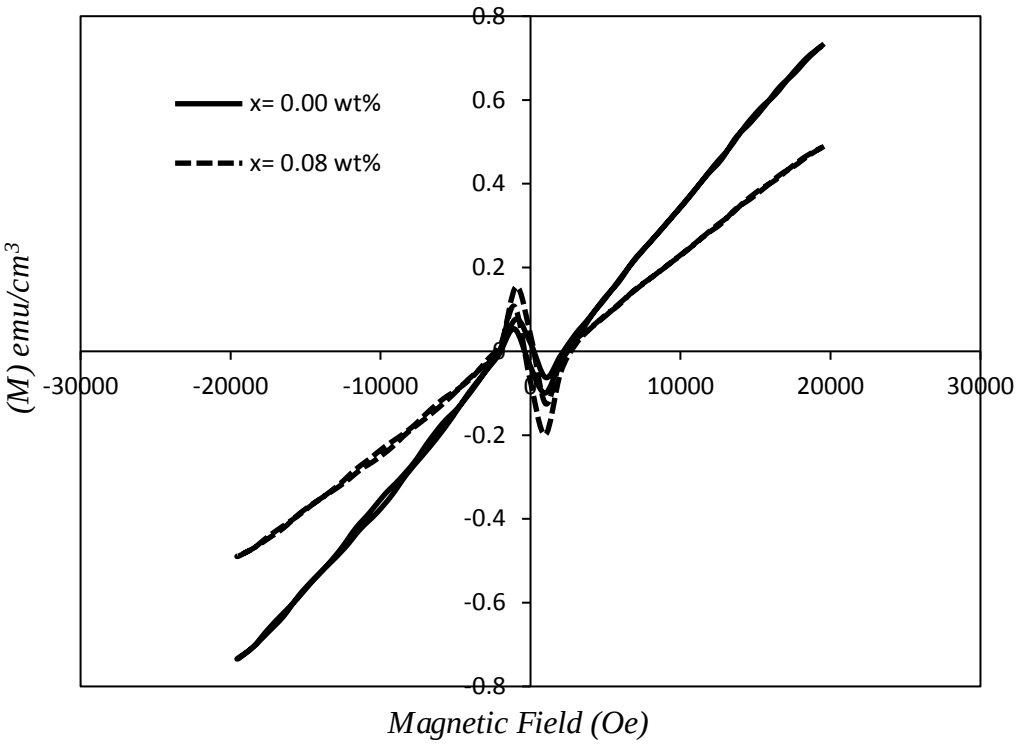

Fig.10: M-H hysteresis loop for $SmBa_2Cu_3O_{7-\delta}$ and $SmBa_2Cu_3O_{7-\delta}$ /$(ZnFe_2O_4)_{0.08}$ at 85 K.

The M-H hysteris loop shows a paramagnetic behavior for both samples. Magnetization shows a linear increase with the magnetic field and even for a field of 20,000)e it does not attain saturation. The M–H curves show small hysteresis at 85 K. This hysteresis is proportional to the critical current density Jc, and usually found in the M–H curves of typical ceramic superconductors. A possible reason for paramagnetism like behavior may be accounted for BaCuO2 impurity phase present in the samples (Topal, 2010).

4. CONCLUSION

EPR measurements for a series of orthorhombic Sm-123/$(ZnFe_2O_4)_x$ composite, with $0.00 \leq x \leq 0.20$ wt% prepared by the solid state reaction method were investigated at different temperatures. In the whole temperature range, *the EPR spectrum comprises* a dominant Cu^{2+} anisotropic pattern described by rhombic g-tensor. The EPR results displayed that the increase of the nanosized $ZnFe_2O_4$, decreased the number of unpaired electrons, activation energy, the paramagnetic susceptibility and the effective magnetic moment up to x= 0.08 wt% due to suppression of the impurity phases (most noticeably $BaCuO_2$) *as* supported by XRD and M-H hysteresis measurements. Those results mean that all of the EPR measurements known to us are not intrinsic to the superconducting phase, but are rather due to small amounts of $BaCuO_2$ typically present in the samples.

REFERENCES:

- Abdeen, W., El-Tahan, A., Roumié, M., Awad, R., Aly, A. A., El-Maghraby, E. M., & Khalaf, A. (2016). Role of improving the physical properties of Sm-123 phase by adding nano-magnetic MnFe2O4. *Journal of Magnetism and Magnetic Materials*, *419*, 354-362.
- Abdeen, W., El Tahan, A., Awad, R., Aly, A. A., El-Maghraby, E. M., & Khalaf, A. (2016). Superconductivity and mechanical properties of SmBa 2 Cu 3 O 7− δ added with nano-crystalline ZnFe 2 O 4. *Applied Physics A*, *122*(6), 574.
- Ashcroft, N. W., & Mermin, N. D. (1976). *Solid State Physics*
- Awad, R., Abou-Aly, A. I., Roumié, M., Mahmoud, S. A., & Barakat, M. M. (2012). Ion beam analysis and EPR studies for GdBa2Cu3− xRuxO7− δ superconducting phase. *Physica C: Superconductivity*, *477*, 74-83.
- Awad, R., Isber, S., Aly, A. A., Abdeen, W., El-Tahan, A., El-Maghraby, E. M., ... & Noureddine, S. (2017, July). EPR studies of SmBa2Cu3O7-δ/MnFe2O4 superconducting composites. In *Journal of Physics: Conference Series* (Vol. 869, No. 1, p. 012033). IOP Publishing.
- Bencini, A., & Gatteschi, D. (2012). *EPR of exchange coupled systems*. Courier Corporation.
- Bowden, G. J., Elliston, P. R., Wan, K. T., Easterling, K. E., Bourdillon, A., Sorrell, C. C., ... & Separovic, F. (1987). EPR and NMR measurements on high-temperature superconductors. *Journal of Physics C: Solid State Physics*, *20*(23), L545.
- Calamiotou, M., Guskos, N., Leventouri, T., Paraskevas, S. M., & Hascicek, Y. S. (1992). EPR Spectra of Bulk Textured Samples of the YBa 2 Cu 3 O x Superconductor. In *Physics and Materials Science of High Temperature Superconductors, II* (pp. 403-411). Springer, Dordrecht.
- Dhage, P., Samokhvalov, A., McKee, M. L., Duin, E. C., & Tatarchuk, B. J. (2013). Reactive adsorption of hydrogen sulfide by promoted sorbents Cu- ZnO/SiO2: active sites by experiment and simulation. *Surface and Interface Analysis*, *45*(5), 865-872.
- Durrell, J. H., Dennis, A. R., Jaroszynski, J., Ainslie, M. D., Palmer, K. G., Shi, Y. H., ... & Cardwell, D. A. (2014). A trapped field of 17.6 T in melt-processed, bulk Gd-Ba-Cu-O reinforced with shrink-fit steel. *Superconductor Science and Technology*, *27*(8), 082001.
- Genossar, J., Shaltiel, D., Zevin, V., Grayevsky, A., & Fisher, B. (1989). Comparison of the ESR spectra in ceramic YBa2Cu3O7-y (1> y> 0) and related phases. *Journal of Physics: Condensed Matter*, *1*(47), 9471.
- Guskos, N., Calamiotou, M., Paraskevas, S. M., Koufoudakis, A., Mitros, C., Gamari- Seale, H., ... & Wabia, M. (1990). On the Influence of Oxygen Deficiency on EPR Spectra of NdBa2Cu3O7− δ. *physica status solidi (b)*, *162*(2), K101-K105.
- Guskos, N., Triberis, G. P., Calamiotou, M., Trikalinos, C., Koufoudakis, A., Mitros, C., ... & Niarchos, D. (1990). Temperature Dependence of the EPR Spectra of GdBa2Cu3O7− δ Compounds in Orthorhombic and Tetragonal Phases. *Physica Status Solidi (b)*, *162*(1), 243-249.
- Guskos, N., Likodimos, V., Londos, C. A., Psycharis, V., Mitros, C., Koufoudakis, A., ... & Metz, H. (1995). Structural, magnetic, and EPR studies of BaCuO2+ x. *Journal of Solid State Chemistry*, *119*(1), 50-61.
- Hoffmann, S. K., & Goslar, J. (1998). Electron spin relaxation of copper (II) ions in diamagnetic crystals. *Applied Magnetic Resonance*, *14*(2-3), 293-303.
- Isber, S., Basma, H., Noureldeen, S., Barakat, M. M., Roumie, M., & Awad, R. (2017). EPR Studies for GdBa 2 Cu 3 O 7− δ Added with Nanosized Ferrite ZnFe 2 O 4 Before and After Irradiation by 3 MeV H+ Ions. *Journal of Superconductivity and Novel Magnetism*, *30*(11), 3315-3320.
- Jones, R., Janes, R., Armstrong, R., Pyper, N. C., Edwards, P. P., Keeble, D. J., & Harrison, M. R. (1990). A combined ESR/X-ray diffraction study of the Y2O3–BaO–CuO phase diagram. *Journal of the Chemical Society, Faraday Transactions*, *86*(4), 675-682.
- Khan, S., Ikram, M., Singh, A., & Singh, R. J. (1997). EPR study of deoxygenated La2CuO4. *Physica C: Superconductivity*, *281*(2-3), 143-148.
- Kuang, M. Q., Wu, S. Y., Yuan, H. K., Wang, L. D., Duan, S. K., Kuang, A. L., & Li, G. Q. (2017). Pseudogap of Ortho-III YBa2Cu3O7− x from Cu EPR investigation. *Journal of Alloys and Compounds*, *690*, 169-175.

- Likodimos, V., Guskos, N., Gamari-Seale, H., Koufoudakis, A., Wabia, M., Typek, J., & Fuks, H. (1996). Copper magnetic centers in oxygen deficient R Ba 2 Cu 3 O 6+ x (R= Nd, Sm): An EPR and magnetic study. *Physical Review B*, *54*(17), 12342.
- Likodimos, V., Guskos, N., Palios, G., Koufoudakis, A., Typek, J., Bojanowski, B., & Wabia, M. (1995). EPR study of localized Cu 2+ paramagnetic ions and Cu 2+ pairs in the oxygen-deficient PrBa 2 Cu 3 O 6+ x and Pr 0.5 R 0.5 Ba 2 Cu 3 O 6+ x (R= Y, Er) compounds. *Physical Review B*, *52*(10), 7682.
- Mohammed, N. H., Abou-Aly, A. I., Awad, R., Ibrahim, I. H., Roumie, M., & Rekaby, M. (2013). Mechanical and electrical properties of (Cu 0.5 Tl 0.5)-1223 phase added with nano-Fe 2 O 3. *Journal of Low Temperature Physics*, *172*(3-4), 234-255.
- Nigro, A., Grimaldi, G., Savo, B., Pace, S., Boffa, M. A., & Cucolo, A. M. (2004). DC transport properties of epitaxial superconducting SmBa2Cu3O7− x films. *Physica C: Superconductivity*, *401*(1-4), 277-281.
- Oh, S. S., Kim, H. S., Ha, H. S., Ko, R. K., Ha, D. W., Lee, H., ... & Yoo, S. I. (2013). Progress in research and development for REBCO coated conductors by reactive co-evaporation. *Progress in Superconductivity and Cryogenics*, *15*(4), 1-5.
- Punnoose, A., & Singh, R. J. (1995). EPR studies of high-Tc superconductors and related systems. *International Journal of Modern Physics B*, *9*(10), 1123-1157.
- Qu, B., Sun, X. D., Li, J. G., Xiu, Z. M., Liu, S. H., & Xue, C. P. (2008). Significant improvement of critical current density in MgB2 doped with ferromagnetic Fe3O4 nanoparticles. *Superconductor Science and Technology*, *22*(1), 015027.
- Raita, O., Popa, A., Toloman, D., Badilita, V., Piticescu, R. R., & Giurgiu, L. M. (2015). Superparamagnetic behavior of ZnFe2O4 nanoparticles as evidenced by EPR. *Journal of Optoelectronics and Advanced Materials*, *17*(9-10), 1314-1318.
- Shi, Y. H., Dennis, A. R., & Cardwell, D. A. (2015). A new seeding technique for the reliable fabrication of large, SmBCO single grains containing silver using top seeded melt growth. *Superconductor Science and Technology*, *28*(3), 035014.
- Song, G. B., Liang, J. K., Liu, F. S., Yang, L. T., Liu, Q. L., Luo, J., & Rao, G. H. (2004). Subsolidus phase relation, crystal structure and superconductivity of the SmBa2− xSrxCu3O7− δ system. *Journal of alloys and compounds*, *381*(1-2), 32-36.
- Topal, U. (2010). Unexpected transport and magnetic properties in Y–Ba–Cu–O superconductors. *physica status solidi (a)*, *207*(5), 1196-1203.
- Troć, R., Janicki, J., Zygmunt, A., Drulis, H., & Niedźwiedź, A. (1994). EPR and magnetic measurements of BaCuO2+ x. *Physica B: Condensed Matter*, *193*(1), 1-9.
- Udomkan, N., Winotai, P., Suryanarayanan, R., & Charoenthai, N. (2005). Structural changes and superconducting properties of Gd1− 2xPrxCaxBa2Cu3O7− δ HTSCs. *Superconductor Science and Technology*, *18*(10), 1294.
- Vier, D. C., Oseroff, S. B., Salling, C. T., Smyth, J. F., Schultz, S., Dalichaouch, Y., ... & Thompson, J. D. (1987). Precautions when interpreting EPR and dc magnetization measurements of high-T c R Ba 2 Cu 3 O 9− x-phase superconducting materials. *Physical Review B*, *36*(16), 8888.
- Weil, J. A., & Bolton, J. R. (2007). *Electron Paramagnetic Resonance: Elementary Theory And Practical Applications*. John Wiley & Sons.
- Xue, R., Dai, H., Chen, Z., Li, T., & Xue, Y. (2013). Effects of Zn doping on crystal structure, Raman spectra and superconductivity of SmBa2Cu3O7− δ systems. *Materials Science and Engineering: B*, *178*(6), 363-367.
- Koksharov, Y. A., Moshchalkov, V. V., Gippius, A. A., Mill, B. V., Zoubkova, Y., Gudenko, S. V., & Mezhuev, A. N. (1991). EPR spectra in R2BaCuO5 (R= Y, Sm, Eu, Gd, Dy, Ho) oxides. Physica C: Superconductivity, 185, 1151-1152.